Loop Analysis and Angle Recovery Based Reactive Power Optimization for Three-Phase Unbalanced Weakly-Meshed Active Distribution Networks

Tianrui Xu, *Student Member, IEEE*, Tao Ding, *Senior Member, IEEE*, Chenggang Mu, *Student Member, IEEE*, Yuntao Ju, *Member, IEEE*, Mohammad Shahidehpour, *Fellow, IEEE*, Chao Zhu, and Yiyang Zhang

***Abstract*—This paper presents a loop analysis and angle recovery (LAAR) based reactive power optimization for three-phase unbalanced and weakly-meshed active distribution networks (ADNs). For each loop, the width first search (WFS) method is used to find the breakpoint bus of each tie line, and then all loops are broken up at these breakpoint buses by disconnecting tie lines, placing added buses, and adding compensation powers, so that the original weakly-meshed ADN can be precisely converted into an equivalent radial ADN. Furthermore, the traditional second-order cone programming can be employed for the equivalent radial networks to find the global optimal solution. However, the compensation powers are not constant values but related to the bus voltages, which are unknown before opening the loops. To address this problem, we design an iterative method to dynamically update the values of compensation powers until the convergence criterion is met. Moreover, the voltage angles are recovered for all loops at each iteration. The effectiveness of the proposed LAAR method is demonstrated by 9 cases, and the results show that the LAAR method can achieve a better convergence performance than the traditional method.**

***Index Terms*—Active distribution networks (ADNs), reactive power optimization (RPO), three-phase unbalanced network, weakly-meshed network, second-order cone programming (SOCP).**

NOMENCLATURE

Indices

i, j, k, n	Indices for buses.
e, f	Indices for branches and VRTs, where e represents the serial number of the branch or VRT with starting bus i and ending bus j, and f represents the serial number of the branch or VRT with starting bus j and ending bus k.
D	Index for three phases. $D \in \{A, B, C\}$.
t	Index for iteration counter.

Sets

G	A connected graph for a meshed ADN.
G'	A connected graph for the radial ADN after breaking up all loops in G.
N	Set of all buses in meshed ADN G.
N'	Set of all buses in radial ADN G'.
E	Set of all branches in meshed ADN G.
E'	Set of all branches in radial ADN G'.
M	Set of all loops in meshed ADN G.
X	Set of all breakpoint buses.
$\pi(j)$	Set of all parents of bus j.
$\delta(j)$	Set of all children of bus j.
$\tau(j)$	Added bus corresponding to the breakpoint bus $j \in X$.
SVC	Set of buses connected SVCs.
cDER	Set of buses connected to conventional DERs.
rDER	Set of buses connected to renewable DERs.
VRT	Set of VRTs.
φ	Set of three phases.

Symbols

$\|.\|$	Magnitude of a complex number.
$\|.\|_\infty$	Infinite norm of a complex vector.
$\overline{(.)}$	Complex conjugate of a complex number.
$(.)^{\mathrm{H}}$	Complex conjugate transpose of a complex vector.
diag(.)	A column vector representation for the main diagonal elements of a matrix.
$\angle(.)$	Phase angle of a complex number.

Variables

I_e	3×1 complex vector represents the current in branch e.

Manuscript received 8 March 2022; revised 28 June 2022; accepted 31 August 2022. Date of publication 5 September 2022; date of current version 22 June 2023. This work was supported in part by the National Natural Science Foundation of China under Grant 51977166, in part by the Natural Science Foundation of Shaanxi Province under Grant 2022JC-19, and in part by the State Grid Shaanxi Electric Power Research Institute-Research through Science and Technology Project on Key technologies of carbon emission accounting of Shaanxi Power System under the background of double carbon under Grant 5226SX21N038. Paper no. TPWRS-00338-2022. *(Corresponding author: Tao Ding.)*

Tianrui Xu, Tao Ding, and Chenggang Mu are with the School of Electrical Engineering, Xi'an Jiaotong University, Xi'an 710049, China (e-mail: tding15@mail.xjtu.edu.cn).

Yuntao Ju is with the College of Information and Electrical Engineering, China Agricultural University, Beijing 100083, China.

Mohammad Shahidehpour is with the Robert W. Galvin Center for Electricity Innovation, Illinois Institute of Technology, Chicago, IL 60616 USA.

Chao Zhu and Yiyang Zhang are with the New Energy Technology Center of the Electric Power Research Institute of State Grid Shaanxi Electric Power Co., Ltd, Xi'an 710048, China.

Color versions of one or more figures in this article are available at https://doi.org/10.1109/TPWRS.2022.3204117.

Digital Object Identifier 10.1109/TPWRS.2022.3204117

V_j	3×1 complex vector represents the nodal voltage of bus j.
S_e	3×1 complex vector represents the power matrix of branch *e*, which equals the product of vector V_j and I_e^{H}.
W_j	3×3 complex matrix represents the product of vector V_j and V_j^{H}.
L_e	3×3 complex matrix represents the product of vector I_e and I_e^{H}.
$S_{j,\text{net}}$	3×1 complex vector represents the apparent power injected from bus j to the feeder.
$S_{j,\text{DER}}$	3×1 complex vector represents the output power from DER at bus j, which equals to $P_{j,DER} + \mathbf{i}Q_{j,DER}$.
$Q_{j,s}$	3×1 vector represents the output power from VRT injected from bus j to the feeder.
$S_{j,\text{inj}}$	3×1 complex vector represents the injection power at bus j.
y_e	Tap ratio of the VRT e.
V_{brk}	$3n_e \times 1$ complex vector represents the breakpoint voltage gap.
θ	Phase angle column vector.
ΔI_{brk}	Incremental current vector.
ΔS_{brk}	Incremental compensation power vector.

Parameters

Z_e	3×3 symmetric matrix represents the three-phase impedance matrix of branch e.
n_b	Number of buses in graph G.
n_e	Number of branches in graph G.
n_l	Number of independent loops in graph G.
$S_{j,\text{Load}}$	3×1 vector represents the apparent load at bus j.
$Q_{j,s}^{\min}$, $Q_{j,s}^{\max}$	3×1 vector represents the minimul/maximum output power of SVC at bus j.
$P_{j,\text{DER}}^{pre}$, $Q_{j,\text{DER}}^{pre}$	3×1 vector represents the predictive active/reactive output power of DER at bus j.
η_j	Power factor angle of DER at bus j.
$\eta_{\min,j}$, $\eta_{\max,j}$	Minimum/maximum power factor of conventional DER at bus j.
$W_{\min,j}, W_{\max,j}$	3×1 vector represents the minimum/maximum squared voltage magnitude limit for bus j.
V_{slack}	3×1 complex vector represents the specified value of the voltage on the slack bus.
S_{sub}	Rated capacity of the substation.
$L_{\max,e}$	3×1 vector represents the square of maximum squared current magnitude limit for branch *e*.
$y_{\min,e}$, $y_{\max,e}$	Minimum/maximum tap ratio of the VRT e.

Acronyms

ADN	Active distribution network.
BVM	Breakpoint voltage mismatch.
DER	Distributed energy resource.
DN	Distribution network.
GA	Genetic algorithm.
LAAR	Loop analysis and angle recovery.
OPF	Optimal power flow.
PFS	Power flow solution.
PSO	Particle swarm optimization.
RPO	Reactive power optimization.
SDP	Semi-definite programming.
SOCP	Second-order cone programming.
SVC	Static var compensators.
VM	Voltage magnitude.
VRT	Voltage regulator transformer.
WFS	Width first search.

I. Introduction

ELECTRICITY generation from fossil fuels has raised concerns about emitting large quantities of carbon dioxide, causing dramatic climate change and unbalancing the global ecology, and global warming has become one of our main environmental problems. Under this background, distributed energy resources (DERs) are developing quickly. Compared with traditional energy sources, DERs, such as photovoltaic power and wind power, generate electricity without emitting carbon, and have a green impact on the global environment. In addition, DERs are able to provide PQ compensation service and voltage regulation. Due to these advantages, more and more DERs are connected to distribution networks (DNs), and along with this trend, conventional passive distribution networks are being transformed into active distribution networks (ADNs) [1]. In the meantime, the installation of DERs can cause significant technical issues such as phase imbalance and capacity limitations [2]. Research on ADNs has been widely conducted, including network planning [3], electricity market [4], topology reconfiguration strategy [5], and optimal power flow (OPF) [6].

The phenomenon of reactive power lack, high line losses, and low voltage in buses are severe in DNs [7]. Reactive power optimization (RPO), which is closely related to the OPF problem, is used to minimize network power losses and prevent voltage violations by dispatching reactive power control devices [8]. The DC OPF is a prevailing tool widely used in transmission networks that linearizes the constraints and makes the problem easier to solve [9], [10]. However, it is not suitable for solving the RPO model in DNs due to the high R/X ratio and incapability of addressing line losses [11]. To address the above challenges, AC OPF should be developed and tested with advanced optimization algorithms to reduce the risk of voltage collapse and enable the effective utilization of existing line capacities [12]. However, the original form of the AC OPF problem is a nonlinear non-convex optimization problem, which can be identified to be an NP-hard problem [13].

One way to solve the non-convex RPO model is using heuristic algorithms, or so-called nature-inspired search algorithms. They have been widely adopted in the field of RPO due to the simplification of the nonconvex NP-hard optimization model and the effectiveness of solving RPO. One approach involves the use of a particle swarm optimization (PSO) algorithm [7]. Reference [14] has achieved low power losses by considering

power electronic transformers in PSO. The premature convergence problem of PSO was successfully solved in [15] by combining the PSO algorithm and chaotic optimization method. In [16], a mathematical model of RPO was established, where the power losses were reduced and voltage quality was improved by the usage of a genetic algorithm (GA). As the GA has a strong global searching capability while an extremely slower speed in the local search, [17] proposed an improved GA integrated with a reduced gradient technique, thus achieving a better computational performance. Reference [18] introduced a modified bat algorithm to confirm the efficiency and robustness of the proposed RPO model by comparing it with other intelligent algorithms. There also have been recent advances in biogeography-based optimization algorithm, simulated annealing algorithm, Tabu search algorithm, artificial immunity algorithm, ant colony optimization, fish-school algorithm, chaos optimization algorithm, etc. [19], [20]. Generally, heuristic algorithms need a too long time to reach a good global solution and have no rigorous mathematical proof for convergence performance.

The second way to handle the nonconvexity of the RPO model is to linearize the nonlinear relationship among voltages, currents, and complex powers [21]. In [22], a linearly-constrained and convergence-guaranteed OPF model was proposed, and the performance was improved compared with DC OPF. Reference [23] presented a linearized active and reactive power coordinated optimization model based on voltage-sensitive load, and the voltage distribution in ADN was improved. However, the exactness and reliability of the linearized model are still questioned. A better study should focus on how to convert the nonlinear non-convex RPO model into a convex model on the premise of accuracy.

The third way to address the non-convex RPO model is focusing on mathematical programming methods as well as their variants (e.g., convex relaxation methods). Reference [24] developed a complete multiphase system model using the primal-dual interior-point method to solve the OPF. In [25], predictor-corrector primal-dual interior-point method was implemented to address nonlinear nonconvex OPF problems, which was sufficiently fast and scalable. Reference [26] solved the RPO with the model based on complementarity theory and the solution based on an interior point filter algorithm, which guaranteed the computational performance. A challenging problem is that in algorithms such as [26], the RPO model is still nonconvex, which makes them easy to fall into the local optimum during the searching process. To address this challenge, convex relaxation was developed. In [27], the OPF was formulated as a quadratically constrained quadratic program which can be approximated by semi-definite programming (SDP). Reference [28] suggested solving the Lagrange dual equivalent form of the OPF problem, which was a convex SDP and can be solved in polynomial time. Similar SDP relaxations also can be found in [29], [30], [31]. In [32], a second-order cone programming (SOCP) relaxation can be derived by relaxing the quadratic equality constraints into inequality constraints. It also proved that the SOCP relaxation of the original nonconvex problem was exact for radial networks. However, the algorithms mentioned above can only deal with the radial DNs or ADNs.

Conventionally, in order to meet electricity demands under the required reliability indices, DNs were designed in a mesh-constructed but operated in a radial way [33], suggesting that DNs typically have a radial structure in operation. However, several researchers have focused on weakly-meshed structures since they allowed the system to operate with lower losses [34], as well as avoiding power interruptions when a single fault occurred in the loop [35], [36]. Reference [37] proposed a method based on SDP to find a global solution to the OPF problem, and the SDP relaxation is exact on certain meshed networks. In [38], phase shifters were installed in order to convert the nonconvex OPF problem into a simpler problem. However, the change of network infrastructure is infeasible in most DNs due to its high construction cost and low reliability. Reference [39] presented a method based on a complex power compensation and branch flow conic formulation to solve the OPF problem, where the compensation power was calculated through the voltage sensitivity. However, its computational performance is challenged. Meanwhile, the voltage sensitivity is difficult to extend to three-phase unbalanced ADNs, to our best knowledge, there is no paper that has reported the application of voltage sensitivity to OPF problems in three-phase unbalanced ADNs. In order to address the RPO model for three-phase unbalance ADNs, this paper proposes an iterative method that has the following contributions:

1) Since the traditional SOCP cannot directly solve weakly-meshed ADNs, the loop-breaking operation is employed by using the width first search (WFS) method to find the breakpoint bus of the tie line in each loop, and then all loops are broken up at breakpoint buses. Then, the original three-phase unbalanced weakly-meshed ADN can be precisely converted into an equivalent three-phase unbalanced radial ADN by adding compensation powers at terminal buses of tie lines. However, compensation powers are unknown before the loop-breaking operation, which may disobey Kirchhoff's laws and fail to find a feasible solution. To address this problem, we designed an iterative method by calculating the incremental compensation powers in each step.
2) Ref. [39] computes compensation powers by using voltage sensitivity, including matrix inversions and large-scale linear equations. In contrast, the proposed method is based on loop analysis, which only needs matrix multiplication operations, so the computational performance is significantly improved.
3) The phase angle of three-phase nodal voltages cannot be obtained directly from the solution of the SOCP model in the radial ADNs after the loop-breaking operation, so the loop analysis is still not precise. To address this problem, we propose a phase angle recovery strategy to precisely obtain the three-phase complex nodal voltage.

The remainder of this paper is organized as follows. Section II describes the details of the proposed loop analysis and angle recovery (LAAR) method, including the transformation from weakly-meshed networks to radial networks by loop breaking operations, the RPO model in radial ADNs, and complex nodal voltage recovery, and the injection compensation power

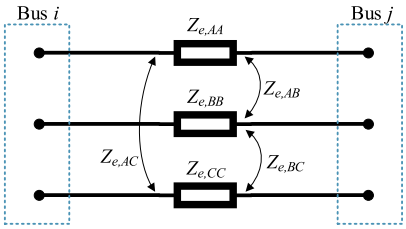

Fig. 1. Structure of a three-phase three-wire line section.

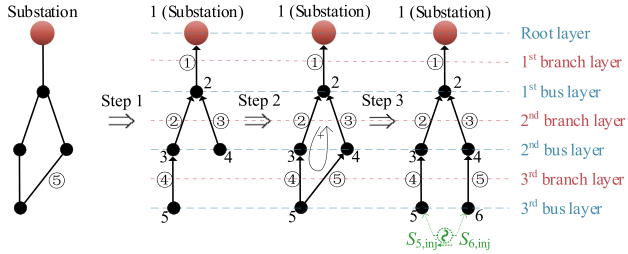

Fig. 2. Loop breaking operation in a 5-buses network.

calculation procedure. Numerical simulations are presented in Section III, and a conclusion is drawn in Section IV.

II. Loop Analysis and Angle Recovery Based Iterative Method for Reactive Power Optimization

When considering balanced situations, we usually assume the whole ADN to be single-phase. But under unbalanced situations, we assume that each element, including line, bus, load, and DER has a three-phase structure. Fig. 1 depicts a three-phase three-wire line section e connected between bus i and bus j, where line parameters can be determined by Kron's method. A 3×3 sized symmetric matrix Z_e of the line segment e can be expressed as

$$Z_e = \begin{bmatrix} Z_{e,AA} & Z_{e,AB} & Z_{e,AC} \\ Z_{e,AB} & Z_{e,BB} & Z_{e,BC} \\ Z_{e,AC} & Z_{e,BC} & Z_{e,CC} \end{bmatrix} \tag{1}$$

where $Z_{e,AA}$, $Z_{e,BB}$, and $Z_{e,CC}$ are the self-impedance of phase A, B, and C, respectively. $Z_{e,AB}$, $Z_{e,AC}$, and $Z_{e,BC}$ are the mutual impedance between phases A and B, A and C, B and C, respectively.

A. The Operation of Breaking Up Loops

Let a meshed DN with n_b buses, n_e branches and n_l independent loops be represented by a connected graph $G = (N, E, M)$. Then we have $n_e = n_b - 1 + n_l$.

The operation of breaking up all loops in G is summarized in the following steps:

Step 0: Index all tie lines starting from the number of $n_e + 1$.

Step 1: Temporarily make the mesh DN radial by removing all tie lines. In this radial DN, all buses can be divided into several layers, and the layer number of one bus is equal to the length of the shortest path from itself to the root bus. Numbering the buses and branches in each layer using the WFS method [40]. For each branch, define the bus near to the root bus as the parent, and the bus far from the root bus as the child. Let $\pi(j)$ be the set of parents of bus j and $\delta(j)$ be the set of children of bus j.

Step 2: After all buses in G have been indexed and divided into several layers by the WFS method, reconnect the tie line so that the temporary radial DN is recovered to the original meshed DN. The direction of a branch is defined from a large terminal bus number to a small terminal bus number, and the direction of a loop is defined as the direction of the tie line it contains.

Step 3: Define the terminal bus of the tie line with the larger number of the layers as the breakpoint bus. Disconnect the tie line originally connected to the breakpoint bus, and place an added bus next to the breakpoint bus $\forall j \in X$. Then connect the tie line from the disconnection to the added bus. To maintain the equivalence between the original meshed network and the radial network, the breakpoint bus in the radial network inherits the original load and DER of the breakpoint bus in the original meshed network, which means there is no power flow in or out of the added bus. To compensate the power flowing through the tie line, add compensation powers $S_{j,inj}$ into bus $\forall j \in X$ and $S_{\tau(j),inj}$ into added bus $\tau(j)$, where $S_{j,inj}$ and $S_{\tau(j),inj}$ are equal in value but opposite in direction. Note that the compensation powers arethe unknown in a prior. According to the voltage relationship, the nodal voltage of bus j and $\tau(j)$ should be equal for both magnitude and phase angle to the original meshed network, and this relationship remains unchanged after all loops are broken up.

As all loops in G are broken up, the set of loops M is turned to aan empty set. The set of branches remains unchanged, and the number of added buses is equal to n_l, so $N' = \{1, 2, \ldots, n_b, n_b + 1, \ldots, n_b + n_l\}$ is the new set of buses. Thus, the original meshed graph $G = (N, E, M)$ is precisely converted into a new radial graph $G' = (N', E)$. In this graph G', branch e connects an ordered pair $(i, j) \in E$ of buses where bus i lies between substation and bus j, i.e., in this notation $(i, j) \in E$ while $(j, i) \notin E$.

For example, the operation of breaking up loops in a simple meshed DN with $n_b = 5$, $n_e = 5$, and $n_l = 1$, is shown in Fig. 2. The tie line of the only loop is branch 5. According to the definition of breakpoint bus, bus 5 has the larger number of layers in the two-terminal buses of branch 5, so the breakpoint bus of the loop is bus 5. The original meshed network can be equivalently converted into a radial structure by disconnecting branch 5, placing an added bus 6 next to bus 5, and then reconnecting branch 5 to bus 6.

B. Reactive Power Optimization Model for Three-Phase Unbalanced Radial Active Distribution Networks

Since we have transformed a meshed network G into a radial network G' by breaking up loops, the RPO model for three-phase radial ADN can be used for graph G', which can be formulated

as

$$\min \sum_{e\in E}\sum_{D\in\{A,B,C\}} R_{e,D}\left|I_{e,D}\right|^2 \tag{2a}$$

$$W_j = W_i + (S_e Z_e^{\mathrm{H}} + Z_e S_e^{\mathrm{H}}) - Z_e L_e Z_e^{\mathrm{H}}, \forall e \in E \tag{2b}$$

$$S_{j,\mathrm{net}} = \mathrm{diag}\left(\sum_{k\in\delta(j)} S_f - (S_e - Z_e L_e)\right), \forall j \in N' \tag{2c}$$

$$S_{j,\mathrm{net}} = S_{j,DER} + \mathbf{i}Q_{j,s} + S_{j,\mathrm{inj}} - S_{j,\mathrm{Load}}, \forall j \in N' \tag{2d}$$

$$S_{j,\mathrm{inj}} + S_{\tau(j),\mathrm{inj}} = \mathbf{0}, \forall j \in X \tag{2e}$$

$$\mathrm{diag}(L_e) \le L_{\max,e}, \forall e \in E \tag{2f}$$

$$W_{\min,j} \le \mathrm{diag}(W_j) \le W_{\max,j}, \forall j \in N' \tag{2g}$$

$$0 \le S_{1,\mathrm{net}} \le S_{\mathrm{sub}} \tag{2h}$$

$$W_1 = V_{\mathrm{slack}} V_{\mathrm{slack}}^{\mathrm{H}} \tag{2i}$$

$$Q_{j,s}^{\min} \le Q_{j,s} \le Q_{j,s}^{\max}, \forall j \in SVC \tag{2j}$$

$$P_{j,DER}^{\min} \le P_{j,DER} \le P_{j,DER}^{\max}, \forall j \in cDER \tag{2k}$$

$$Q_{j,DER}^{\min} \le Q_{j,DER} \le Q_{j,DER}^{\max}, \forall j \in cDER \tag{2l}$$

$$\frac{\eta_{\min,j}}{\sqrt{1-(\eta_{\min,j})^2}} Q_{j,DER} \le P_{j,DER} \le \frac{\eta_{\max,j}}{\sqrt{1-(\eta_{\max,j})^2}} Q_{j,DER}, \quad \forall j \in cDER \tag{2m}$$

$$0 \le P_{j,DER} \le P_{j,DER}^{pre}, \forall j \in rDER \tag{2n}$$

$$-Q_{j,DER}^{pre} \le Q_{j,DER} \le Q_{j,DER}^{pre}, \forall j \in rDER \tag{2o}$$

$$Q_{j,DER}^{pre} = \eta_j P_{j,DER}, \forall j \in rDER \tag{2p}$$

$$\left\| \frac{2W_k(g,h)}{W_k(g,g)-W_k(h,h)} \right\|_2 \le W_k(g,g) + W_k(h,h), \quad \forall k \in N', \forall g,h \in \{1,2,3\} \tag{2q}$$

$$\left\| \frac{2L_e(g,h)}{L_e(g,g)-L_e(h,h)} \right\|_2 \le L_e(g,g) + L_e(h,h), \quad \forall e \in E, \forall g,h \in \{1,2,3\} \tag{2r}$$

$$\left\| \frac{2S_e(g,h)}{W_k(g,g)-L_e(h,h)} \right\|_2 \le W_k(g,g) + L_e(h,h), \quad \forall e \in E, \forall g,h \in \{1,2,3\} \tag{2s}$$

In the RPO model (2a)–(2s), (2a) represents the objective function, which minimizes total line losses. (2b) is the power flow equation that describes the voltage drop related to the branch power flows, following Kirchhoff's voltage law. (2c) and (2d) represents the power balance equation at each node which follows Kirchhoff's current law, so that the power coming into a node equals the power going out. (2e) is the injected compensation power equation at each pair (i.e., breakpoint bus and its added bus). (2f) and (2g) are the limits of branch current magnitudes and voltage magnitudes (VMs), respectively. (2h) is the limit of substation capacity. (2i) represents that the voltage of the substation is set to a fixed value. (2j) is the limit of output power of static var compensators (SVCs). (2k)–(2m) are the operational constraints of conventional DERs [41]. (2n)–(2p) are the operational constraints of renewable DERs, where the superscript *pre* denotes the predictive value. According to [42], power electrical devices or conventional rotary motor interfaces of DERs can adjust active power and reactive power respectively. Herein, the output reactive power of renewable DERs can be continuously adjusted in the interval [0, $Q_{j,DER}^{pre}$], where $Q_{j,DER}^{pre}$ is jointly controlled by the predictive value of active output power $P_{j,DER}^{pre}$ and power factor η_j. (2q)–(2s) are second-order cones obtained from the positive semi-definite convex constraint, and the detailed relaxation process is shown in [43], [44].

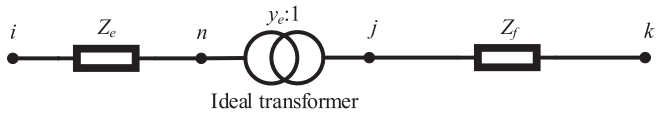

Fig. 3. Equivalent circuit of a VRT.

A voltage regulator transformer (VRT) can be modeled as a three-phase wye-wye connected ideal transformer with a ratio of y_e and in series with an impedance (see Fig. 3) according to [45], whose mathematical model is shown in (3a)–(3d).

$$W_n = W_i + \left(S_e Z_e^{\mathrm{H}} + Z_e S_e^{\mathrm{H}}\right) - Z_e L_e Z_e^{\mathrm{H}}, \forall e \in VRT \tag{3a}$$

$$W_n = y_e W_j \tag{3b}$$

$$y_e L_e = \sum_{k\in\delta(j)} L_f \tag{3c}$$

$$S_{j,\mathrm{net}} = \mathrm{diag}\left(\sum_{k\in\delta(j)} S_f - (S_e - Z_e L_e)\right), \forall e \in VR \tag{3d}$$

According to [46], the convex forms of (3b) and (3c) are derived as (4) and (5), respectively.

$$\begin{cases} \mathrm{diag}(W_n) \ge y_{\min,e}\mathrm{diag}(W_j) + y_e W_{\min,j} - y_{\min,e} W_{\min,j} \\ \mathrm{diag}(W_n) \ge y_{\max,e}\mathrm{diag}(W_j) + y_e W_{\max,j} - y_{\max,e} W_{\max,j} \\ \mathrm{diag}(W_n) \le y_{\max,e}\mathrm{diag}(W_j) + y_e W_{\min,j} - y_{\max,e} W_{\min,j} \\ \mathrm{diag}(W_n) \le y_{\min,e}\mathrm{diag}(W_j) + y_e W_{\max,j} - y_{\min,e} W_{\max,j} \end{cases}, \quad \forall e \in VRT \tag{4}$$

$$\begin{cases} \mathrm{diag}\left(\sum_{k\in\delta(j)} L_f\right) \ge y_{\min,e}\mathrm{diag}(L_e) \\ \sum_{k\in\delta(j)} \mathrm{diag}(L_f) \ge y_{\max,e}\mathrm{diag}(L_e) \\ \quad + y_e L_{\max,e} - y_{\max,e} L_{\max,e} \\ \sum_{k\in\delta(j)} \mathrm{diag}(L_f) \le y_{\max,e}\mathrm{diag}(L_e) \\ \sum_{k\in\delta(j)} \mathrm{diag}(L_f) \le y_{\min,e}\mathrm{diag}(L_e) \\ \quad + y_e L_{\max,e} - y_{\min,e} L_{\max,e} \end{cases}, \quad \forall e \in VRT \tag{5}$$

In summary, the RPO model for three-phase radial ADN is written as

$$\min \sum_{e\in E}\sum_{D\in\{A,B,C\}} R_{e,D}\left|I_{e,D}\right|^2 \tag{6}$$

$$\text{s.t.} \quad \text{(2b)–(2s), (3a), (3d), (4), (5)} \tag{7}$$

The decision variables of the SOCP model (6), (7) are the elements in matrices ($Q_{j,s}$, $S_{j,DER}$, $S_{j,inj}$, y_e, W_k, L_e, S_e). Before solving the RPO model (6), (7), the value of $S_{j,inj}$ is unknown. An iterative method is designed to address this problem. Assume that we have $S_{j,inj}^{(t)} = S_{\tau(j),inj}^{(t)} = 0, t = 1$ in (2e), where the superscript (t) denotes the iteration counter, and $t = 1$ is the initial step. Note that when we set the value of $S_{j,inj}$ to be zero, the voltage of bus $\tau(j)$ is equal to bus $i \in \pi(j)$.

C. Angle Recovery of Three-Phase Complex Nodal Voltage

After solving the RPO model (6), (7), the three-phase nodal VMs at bus j can be obtained by (8).

$$\begin{cases} \left|V_{j,A}^{(t)}\right| = \sqrt{W_j^{(t)}(1,1)} \\ \left|V_{j,B}^{(t)}\right| = \sqrt{W_j^{(t)}(2,2)} \\ \left|V_{j,C}^{(t)}\right| = \sqrt{W_j^{(t)}(3,3)} \end{cases}, \forall j \in N' \tag{8}$$

However, the phase angle of nodal voltage cannot be obtained from the result of the RPO model (6), (7). Ref. [38] proved that the angle recovery condition always holds for radial networks. The meshed network has been converted into the radial network by the operation of breaking up loops. According to this theory, phase angles can be computed by solving the linear system which is discussed in this part.

Define the $3(n_b + n_l) \times 3n_e$ incident matrix C of G' by

$$C(i,e) = \begin{cases} \mathbf{1}, & \text{if branch } e \text{ leaves bus } i \\ -\mathbf{1}, & \text{if branch } e \text{ enters bus } i \\ \mathbf{0}, & \text{otherwise} \end{cases} \tag{9}$$

$$\mathbf{1} = \begin{bmatrix} 1 & 0 & 0 \\ 0 & 1 & 0 \\ 0 & 0 & 1 \end{bmatrix}, -\mathbf{1} = \begin{bmatrix} -1 & 0 & 0 \\ 0 & -1 & 0 \\ 0 & 0 & -1 \end{bmatrix}, \mathbf{0} = \begin{bmatrix} 0 & 0 & 0 \\ 0 & 0 & 0 \\ 0 & 0 & 0 \end{bmatrix} \tag{10}$$

where $\mathbf{1}$, $-\mathbf{1}$, $\mathbf{0}$ are 3×3 diagonal matrices whose elements are all zeros except three elements $1, -1, 0$ in their diagonal positions, respectively, as shown in (10). Each element $C(i,e)$ in matrix C is a 3×3 block matrix, where $C(i,e)$ represents the block matrix of the i^{th} row and e^{th} column in matrix C.

The first three rows of C correspond to bus 1, i.e., the substation bus with a given three-phase nodal voltage $[V_{1,A}, V_{1,B}, V_{1,C}]^{\mathrm{T}} = |V_1|[e^{\mathbf{i}\theta_{1,A}}, e^{\mathbf{i}\theta_{1,B}}, e^{\mathbf{i}\theta_{1,C}}]^{\mathrm{T}}$. By removing the first three rows (corresponding to V_1) and taking the transpose of the matrix C, we obtain the $3n_e \times 3(n_b + n_l - 1)$ reduced incident matrix B, written as

$$B(e,i) = \begin{cases} \mathbf{1}, & \text{if branch } e \text{ leaves bus } i \\ -\mathbf{1}, & \text{if branch } e \text{ enters bus } i \\ \mathbf{0}, & \text{otherwise} \end{cases} \tag{11}$$

Let $\beta \in [-\pi, \pi]^{3n_e}$ be defined as

$$\begin{cases} \beta(3e-2) = \angle(W_i(1,1) - Z_e^{\mathrm{H}}(1,1)S_e(1,1)) \\ \beta(3e-1) = \angle(W_i(2,2) - Z_e^{\mathrm{H}}(2,2)S_e(2,2)), \forall e \in E \\ \beta(3e) = \angle(W_i(3,3) - Z_e^{\mathrm{H}}(3,3)S_e(3,3)) \end{cases} \tag{12}$$

Furthermore, the phase angle vector can be expressed as $\theta^{(t)} = B^{-1}\beta$, and we can recover the three-phase complex nodal voltage at each bus except for the substation bus by (13). As shown in Part A of this section, we have $n_e = n_b + n_l - 1$ and $rank(B) = 3n_e$. Since the submatrix $B_\perp$ is empty, the uniqueness of $\theta^{(t)}$ is guaranteed.

$$\begin{cases} V_{j,A}^{(t)} = \sqrt{W_j^{(t)}(1,1)}\cos(\theta^{(t)}(3j-2)) \\ \qquad + \mathbf{i}\sqrt{W_j^{(t)}(1,1)}\sin(\theta^{(t)}(3j-2)) \\ V_{j,B}^{(t)} = \sqrt{W_j^{(t)}(2,2)}\cos(\theta^{(t)}(3j-1)) \\ \qquad + \mathbf{i}\sqrt{W_j^{(t)}(2,2)}\sin(\theta^{(t)}(3j-1)) \\ V_{j,C}^{(t)} = \sqrt{W_j^{(t)}(3,3)}\cos(\theta^{(t)}(3j)) \\ \qquad + \mathbf{i}\sqrt{W_j^{(t)}(3,3)}\sin(\theta^{(t)}(3j)) \end{cases}, \quad \forall j \in N', j \neq 1 \tag{13}$$

D. Compensation Powers Using Loop Analysis Theory

Loop analysis is an efficient network analysis tool for radial or weakly meshed DNs. To our best knowledge, this method was only used for the power flow analysis [47]. In this paper, we will employ this theory to the RPO for three-phase unbalanced weakly-meshed ADNs. For each step, all the loops of the ADNs are broken up and then the corresponding compensation powers are added by the following steps. Define the $3n_l \times 3n_e$ loop-branch incident matrix LB by

$$LB(l,e) = \begin{cases} \mathbf{1}, & \text{if loop } l \text{ \& branch } e \text{ are in the same direction} \\ -\mathbf{1}, & \text{if loop } l \text{ \& branch } e \text{ are in the opposite direction} \\ \mathbf{0}, & \text{otherwise} \end{cases} \tag{14}$$

where $\mathbf{1}$, $-\mathbf{1}$, $\mathbf{0}$ are matrices shown in (10). The direction of branches and loops is defined in Part A of this section. Every element $LB(l,e)$ in matrix LB is a 3×3 block matrix, and $LB(l,e)$ represents the block matrix of the l^{th} row and e^{th} column of matrix LB.

For instance, the LB matrix of the meshed DN on the left in Fig. 2 can be formulated as (15) shown at the bottom of the next page.

Calculating $3nl \times 3nl$ breakpoint impedance matrix (Thevenin equivalent impedance) Z_{loop} based on the multi-port

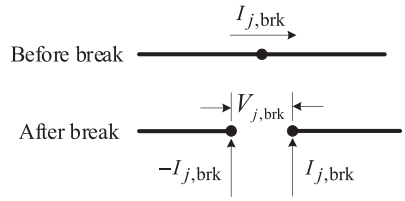

Fig. 4. Scheme diagram of breakpoint voltage.

compensation principle [40] as

$$Z_{loop} = LB \times Z_b \times LB^{\mathrm{T}} \tag{16}$$

where the diagonal elements of matrix Z_b are all 3×3 block matrices shown in (1). The size of Z_b is thus $3nl \times 3nl$.

Define $V_{j,brk} = V_j^{(t)} - V_{\tau(j)}^{(t)}$ to be the breakpoint voltage (i.e., Thevenin equivalent voltage). As shown in Fig. 4, after we break up bus j in the loop, the current flow through bus j still follows the Kirchhoff's current law, due to the following

$$\Delta I_{\mathrm{brk}} = Z_{loop}^{-1} \times V_{brk} \tag{17}$$

where ΔI_{brk} is the incremental breakpoint current vector. Due to the relationship among power, voltage and current, we have

$$\Delta S_{\mathrm{brk}} = V_{brk} \times \overline{\Delta I_{brk}} \tag{18}$$

For next iteration step, the new value of $S_{j,inj}^{(t+1)}$ and $S_{\tau(j),inj}^{(t+1)}$ can be updated by $S_{j,inj}^{(t+1)} = S_{j,inj}^{(t)} + \Delta S_{brk}$ and $S_{\tau(j),inj}^{(t+1)} = S_{\tau(j),inj}^{(t)} - \Delta S_{brk}$, respectively. The optimization model (6), (7) is repeatedly solved. Note that in each iteration step, the incremental compensation power vector ΔS_{brk} is computed to reduce the infinite norm of breakpoint voltage vector $|V_{j,brk}|_\infty$ until $|V_{j,brk}|_\infty \le \varepsilon, \forall j \in N$. This suggests that the solution of the radial RPO model is valid for the original meshed network. The iterative method based on LAAR shown in Fig. 5 can be described as

1) Initialize the model, including indexing all buses and branches, breaking up all loops, and inputting all parameters.
2) Calculate the breakpoint impedance matrix Z_{loop} of the original weakly-meshed ADN.
3) Set the iteration counter $t = 1$.
4) Set the initial value of compensation power in each breakpoint bus and its added bus as zero: $S_{j,inj}^{(t)} = S_{\tau(j),inj}^{(t)} = 0$, $\forall j \in X$.
5) Solve the radial RPO model (6), (7) using the value of compensation power set in step (4). After this step, the result of nodal voltage matrix $W_j^{(t)}$, $\forall j \in N'$ is obtained.

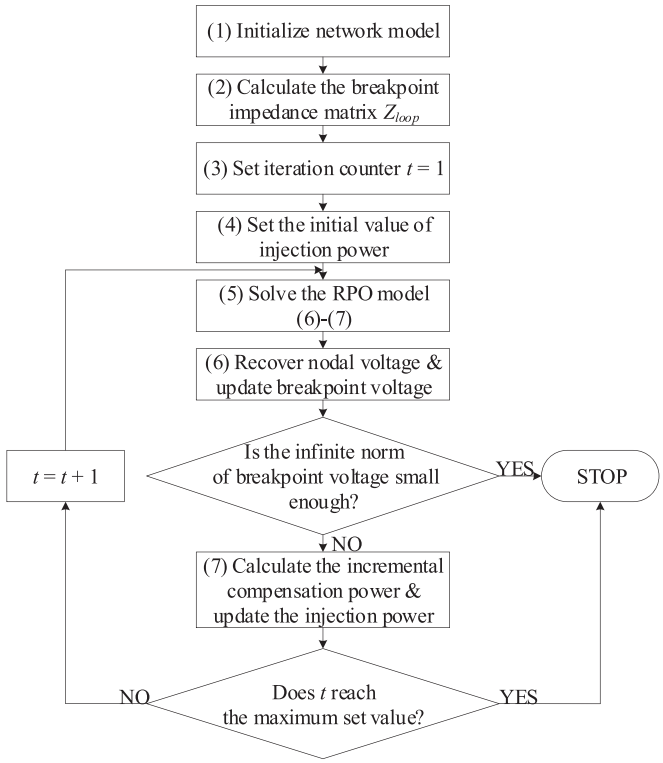

Fig. 5. Flowchart of the iterative method based on LAAR.

6) Recover the angle of three-phase nodal voltage, and update the breakpoint voltage $V_{j,brk}$, $\forall j \in X$. If $|V_{brk}|_\infty < \varepsilon$, $\forall j \in N$, stop the iteration. Otherwise, go to step (7).
7) Calculate the incremental compensation power vector $\Delta \mathrm{S}_{\mathrm{brk}}$ and update the compensation power. If the iteration counter t reaches its maximum set value, stop the iteration. Otherwise, update iteration counter $t = t + 1$, and go back to step (5).
8) Steps (5)–(7) are repeated until the convergence is achieved (the infinite norm of breakpoint voltage vector is small enough).

III. Case Study

In this section, we will analyze the performance of the LAAR method in both balanced and unbalanced cases. Please note that the balance systems can be termed as the special cases of the unbalanced systems with all symmetric topology parameters and balanced injected powers. For balanced situations, we use IEEE 33-bus system [48], IEEE 69-bus system [49], 118-bus system [50], 136-bus system [51], 141-bus system [52], and a real-world ADN with 3623 buses and 4 tie lines (Fig. 6). For unbalanced situations, the modified IEEE 37-bus system,

$$LB = loop\#1 \begin{bmatrix} \overset{(1)}{\begin{bmatrix} 0 & 0 & 0 \\ 0 & 0 & 0 \\ 0 & 0 & 0 \end{bmatrix}} & \overset{(2)}{\begin{bmatrix} -1 & 0 & 0 \\ 0 & -1 & 0 \\ 0 & 0 & -1 \end{bmatrix}} & \overset{(3)}{\begin{bmatrix} 1 & 0 & 0 \\ 0 & 1 & 0 \\ 0 & 0 & 1 \end{bmatrix}} & \overset{(4)}{\begin{bmatrix} -1 & 0 & 0 \\ 0 & -1 & 0 \\ 0 & 0 & -1 \end{bmatrix}} & \overset{(5)}{\begin{bmatrix} 1 & 0 & 0 \\ 0 & 1 & 0 \\ 0 & 0 & 1 \end{bmatrix}} \end{bmatrix} \quad branch \tag{15}$$

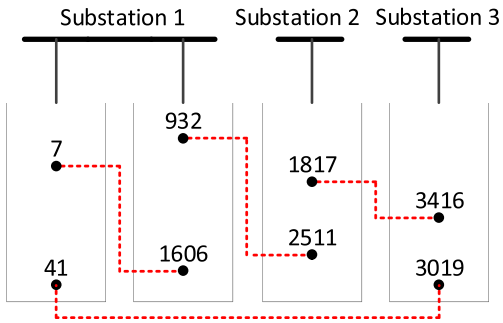

Fig. 6. Topology diagram of the 3623-bus real-world ADN.

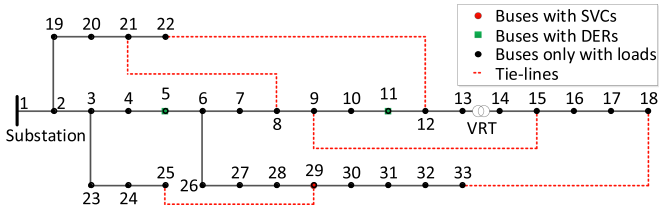

Fig. 7. Grid topology of the modified IEEE 33-bus system.

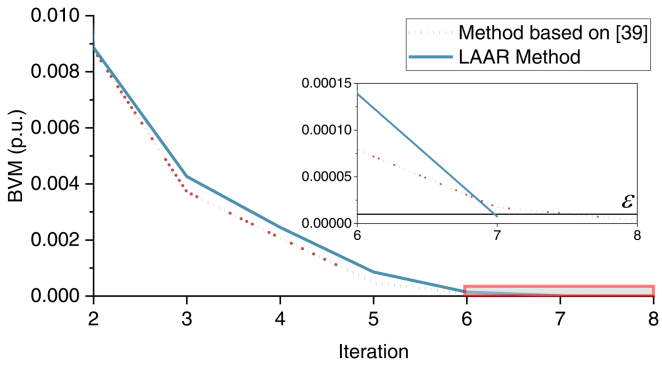

Fig. 8. Convergence of BVM in the modified IEEE 33-bus system.

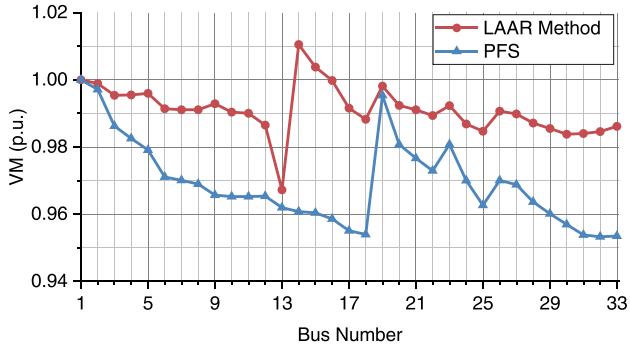

Fig. 9. VMs of the PFS and the LAAR method in the modified IEEE 33-bus system.

IEEE 123-bus system[53] and 3623-bus ADN are used [54]. The 3623-bus ADN has both balanced and unbalanced cases, so we add "B-" and "UN-" before their name in order to make a distinction. We modify all cases mentioned above, including placing tie lines, SVCs, and DERs. Both the LAAR method and the method based on [39] are implemented in MATLAB Version

TABLE I
TOTAL ACTIVE POWER LOSSES (KW)

Cases	PFS	LAAR Method
Modified IEEE 33-bus	123.47	88.34 **(-28.5%)**
Modified IEEE 69-bus	203.79	158.84 **(-22.1%)**
Modified 118zh	909.79	580.03 **(-36.2%)**
Modified 136ma	371.05	258.17 **(-30.4%)**
Modified 141	436.39	98.61 **(-77.4%)**
B-3623	1821.29	1315.86 **(-27.75%)**

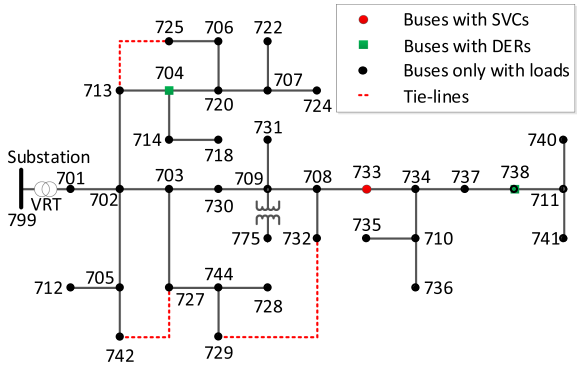

Fig. 10. Topology of the modified IEEE 37-bus system.

2020a and executed on a workstation with Intel Core i7-9700 CPU (3.00GHz) and 16 GB RAM. We solve the optimal model with Gurobi 9.1.2 [55]. A feasibility tolerance of 1.0×10^{-5} is applied to breakpoint voltage mismatch in each case.

A. Balanced Cases

In balanced ADNs, the line impedance, loads and other parameters of different phases are equal, so three-phase systems can be simplified to single-phase systems. Grid topology of the modified IEEE 33-bus system is depicted in Fig. 7, which consists of 33 buses, 32 radial branches, and 5 normally connected tie lines (8–21, 9–15, 12–22, 18–33, 25–29). One VRT is located between bus 13 and 14, whose lower and upper bounds of tap ratios is set as 0.95 p.u. and 1.05 p.u. Base values for power and voltage are 10 MVA and 12.66 kV, respectively. One renewable DER is located at buses 5 with a maximum active output power of 100 kW and the power factor $\eta = 0.9$. One conventional DER is located at bus 11 with a maximum active output power of 100 kW and the power factor $\eta_{\max} = 0.95$, $\eta_{\min} = 0.9$. One SVC is located at bus 29 with a maximum reactive output power of 90 kvar.

Both the LAAR method and the method in [39] are tested. Between the two methods, the maximum errors of voltage magnitudes and phase angles are 6.1×10^{-8} p.u. and 2.8×10^{-7} rad, respectively. The maximum errors of active and reactive branch power flows are 5.5×10^{-7} p.u. and 1.0×10^{-8} p.u. The maximum error of output reactive power of DERs is 1.1×10^{-6}. Errors above show that the two methods can achieve the same

TABLE II
COMPARISON OF COMPUTATIONAL PERFORMANCE

Cases	Number of conic constraints	The method [39]			LAAR method		
		Number of iterations	Computational time of compensation power (s)	Total computational time (s)	Number of iterations	Computational time of compensation power (s)	Total computational time (s)
IEEE 33-bus	37	8	2.1498	13.7517	7	0.0088	10.1626
IEEE 69-bus	73	6	3.4949	13.4479	6	0.0060	12.3229
118zh	131	4	4.3129	15.6505	4	0.0043	12.2301
136ma	145	6	7.8108	27.4507	6	0.0067	19.6009
141	144	3	4.2593	13.0293	3	0.0049	9.1006
B-3623	3625	3	432.8511	854.6073	3	0.0064	517.2615

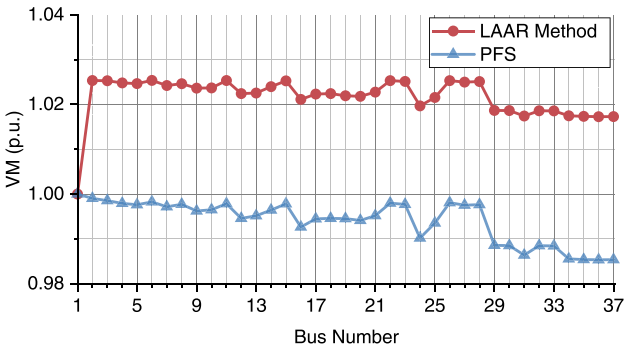

(a) VMs of the PFS and the LAAR method in phase A

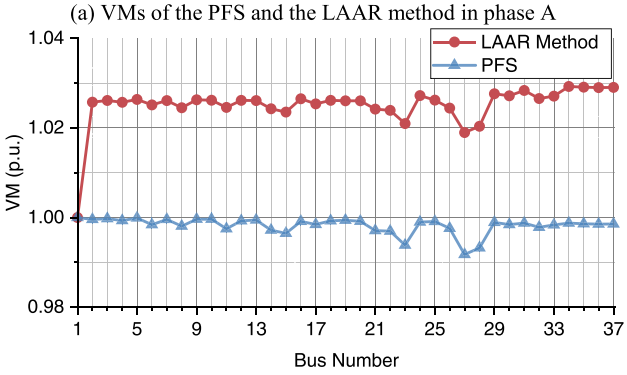

(b) VMs of the PFS and the LAAR method in phase B

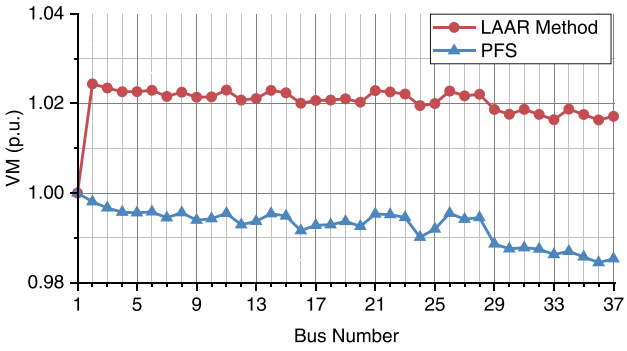

(c) VMs of the PFS and the LAAR method in phase C

Fig. 11. VMs of the PFS and the LAAR method in the modified IEEE 37-bus system.

precision. Furthermore, Fig. 8 shows the convergence curves of the breakpoint voltage mismatch (BVM), i.e., $|V_{brk}|_\infty$ for the two methods. It can be concluded that the convergence criterion is reached after 8 iterations for the method [39] and 7 iterations for the LAAR method. The gaps of BVM between the two methods keeps extremely small values, indicating that the two methods have a similar convergence performance in this small-scale balanced system.

TABLE III
COMPARISON OF TOTAL ACTIVE POWER LOSSES (KW)

Cases	PFS	LAAR Method
Modified IEEE 37-bus	28.57	15.63 **(-45.29%)**
Modified IEEE 123-bus	174.11	87.90 **(-49.52%)**
UN-3623	1819.11	1331.74 **(-26.79%)**

To quantify the voltage profiles of the LAAR method, we compute the power flow solution (PFS) of the original DN [56], i.e., without DERs and SVCs, and set the tap ratio of the VRT to 1. The results of nodal VMs are shown in Fig. 9. Total VM drops are 0.05396 p.u. for the LAAR method, and 0.13485 p.u. for the PFS, where PFS is nearly 1.5 times larger than LAAR method.

Similarly, total active power losses of the PFS and LAAR method in different test cases are shown in Table I. As we can see, the LAAR method can achieve much less active power losses. For example, the active power losses of the LAAR method are reduced by 28.5% compared with the PFS in the modified IEEE 33-bus system. This is because the active power losses are related to the current flowing through the branch resistance that is associated with the voltage drop. As a result, the larger total VM drop will result in larger active power losses. In this term, the RPO is to reduce the overall active power losses, thus reducing the voltage drops of the ADN as well.

Computational performance of the two methods is compared on different cases, which is shown in Table II. Computational time in Table II is based on the average time taken after 10 runs. For most cases, the number of iterations for the two methods is the same. However, in the modified IEEE 33-bus system, the LAAR method needs fewer iterations than the method [39]. It is also worth mentioning that in each iterative step, both the LAAR method and the method [39] need to calculate the compensation power, but the corresponding ideas are different, which therefore lead to different computational time. The method [39] computes the compensation power using a voltage sensitivity matrix, which requires matrix inverse operations or solving large-scale

TABLE IV
PERFORMANCE OF COMPUTATIONAL EFFICIENCY

Test Systems	Number of loops (tie lines)	Number of iterations	Total computational time (s)	Computational time of compensation powers (s)	Number of conic constraints
IEEE 37-bus	0	1	6.5846	0.0015	648
	1 (727-742)	7	40.2050	0.0123	666
	2 (729-732, 727-742)	9	51.8897	0.0126	684
	3 (713-725, 729-732, 727-742)	12	91.7973	0.0186	702
IEEE 123-bus	0	1	17.5989	0.0011	2124
	1 (85-114)	3	49.3639	0.0065	2142
	3 (50-65, 52-96, 85-114)	4	69.5722	0.0107	2178
	5 (50-65, 52-96, 85-114, 48-250, 61-88)	4	69.5827	0.0102	2214
UN-3623	0	1	1895.6470	0.0871	54318
	2 (7-1606, 932-2511)	2	3544.7871	0.1614	54354
	4 (7-1606, 932-2511, 1817-3416, 41-3019)	3	5754.2294	0.2651	54390

linear equations in each step. In contrast, the LAAR method only needs matrix multiplication operations. It can be observed from Table II that the LAAR method requires less computational time than the method [39], especially in large-scale ADNs. For example, the total computational time in B-3623 system with 4 loops is reduced by 39%. The main reason is caused by the computation of the compensation power. Compared with that of the method [39], the computational time by the LAAR method can be significantly reduced from 432.8511 s to 0.0064 s. Besides, the LAAR method needs less iterations than the method [39], which will further reduce the computational time from 11.60 s (i.e., 13.7517 s - 2.1498 s) to 10.15s (i.e., 10.1626 s - 0.0088 s). The efficiency of the LAAR method is improved by 12.48%.

B. Unbalanced Cases

For unbalanced ADNs, the three-phase structure of the system is fully considered in the LAAR method. The line impedance, load, and other parameters are expressed in three-phase forms. However, the method [39] was guided by the voltage sensitivity matrix, which was unable to handle three-phase unbalanced ADNs. The proposed RPO model built by the three-phase structure of ADNs can be suitable for three-phase unbalanced ADNs using the LAAR method. In this part, we will use three-phase unbalanced cases, including the modified IEEE 37-bus system, modified IEEE 123-bus system, and UN-3623-bus ADN to show the effectiveness of the LAAR method.

The grid topology of the modified IEEE 37-bus system is shown in Fig. 10, consisting of 37 buses, 36 radial branches, and 3 normally connected tie lines (713-725, 727-742, 729-732) that make it mesh. One VRT is located between bus 799 and bus 701, whose lower and upper bounds of tap ratio is set as 0.95 p.u. and 1.05 p.u. The base values for power and voltage are 10 MVA and 4.8 kV, respectively. One renewable DER is located at buses 704 with a maximum active output power of 80 kW per phase and the power factor $\eta = 0.9$. One conventional DER is located at bus 738 with a maximum active output power of 80 kW per phase and the power factor $\eta_{\max} = 0.95$, $\eta_{\min} = 0.9$. One SVC is located at bus 733 with a maximum reactive output power of 72 kvar per phase. Note that the output power of DERs and SVC can be adjusted independently for each phase.

The VMs of each phase of the PFS and the LAAR method are shown in Fig. 11. The three-phase VMs are different due to the unbalanced nature of the test case. Total VM drops of the three phases are 0.0219 p.u. in the LAAR method, and 0.0789 p.u. in PFS. Consistent with the balanced case, the LAAR method has lower total VM drop than PFS. Total active power losses are shown in Table III. The active power losses of the LAAR method is lower than PFS, which has the same trend as total VM drops. This means that in three-phase unbalanced ADNs, the active power losses are also associated with voltage drops.

In order to investigate the scalability and the number of loops on the computational performance of the LAAR method for the unbalanced ADNs, we choose three test systems under different conditions. The results can be found in Table IV. Computational time in Table IV is based on the average time taken after 10 runs. The number of loops is 0 means that the network is radial. For each system, when the number of the loops increases, the number of iterations is normally increased. Thus, the total computational time and the computational time of compensation power will be increased as well. Moreover, the number of iterations and the computational time takes on a roughly linear relationship. In particular, the computational time of compensation power is usually very short no matter how the number of loops changes, i.e., always less than 0.3 s. As a result, the total computational time is mainly affected by the second-order cone programming for the reactive power optimization due to a large number of conic constraints. For UN-3623 system, the number of conic constraints is about 54390 when the number of loops is 4, and the total computational time is 5754.2294 s. As comparison, there are 3625 conic constraints in the balanced system B-3623. Thus, the computational time for UN-3623 is increased by 5237 s. Straightforwardly, with the increase of the system scale, the number of conic constraints will be increased significantly and the computational time is increased accordingly. Last but not the least, we can find that for the same system, the number of conic constraints increases only slightly with increasing the number of loops. However, the computational time will increase significantly because the larger number of loops will cause more

iterations. Therefore, the scale and the number of loops are two main reasons for the computational time of RPO for three-phase unbalanced ADNs.

IV. Conclusion

We have studied an RPO model for three-phase unbalanced and weakly-meshed ADNs. Based on LAAR, a weakly-meshed ADN can be precisely converted into a radial ADN by breaking up loops in breakpoint buses, and the compensation power and angle recovery are calculated in each iteration step. The LAAR method was tested in both balanced and unbalanced situations. In balanced situations, the LAAR method has a better computational performance than traditional method. In unbalanced situations where the traditional methods cannot handle the three-phase structure, the LAAR method is able to find the global optimal solution. Also, we find that the scale and the number of loops mainly affect the computational time. Future work will investigate the impact of uncertainties, such as distributed generation, on the proposed model and method.

References

[1] W. Zheng, W. Wu, B. Zhang, H. Sun, and Y. Liu, "A fully distributed reactive power optimization and control method for active distribution networks," *IEEE Trans. Smart Grid*, vol. 7, no. 2, pp. 1021–1033, Mar. 2016.

[2] I. A. Ibrahim and M. J. Hossain, "Low voltage distribution networks modeling and unbalanced (optimal) power flow: A comprehensive review," *IEEE Access*, vol. 9, pp. 143026–143084, 2021.

[3] Q. S. Cui, X. M. Bai, S. Z. Zhu, and N. Li, "ADN multi-objective planning considering collaborative optimization of rdg and GAEP," in. *Proc. IEEE Int. Conf. Power Syst. Technol.*, 2016, pp. 1–7.

[4] L. Bai, J. Wang, C. Wang, C. Chen, and F. Li, "Distribution locational marginal pricing (DLMP) for congestion management and voltage support," *IEEE Trans. Power Syst.*, vol. 33, no. 4, pp. 4061–4073, Jul. 2018.

[5] S. Golshannavaz, S. Afsharnia, and F. Aminifar, "Smart distribution grid: Optimal day-ahead scheduling with reconfigurable topology," *IEEE Trans. Smart Grid*, vol. 5, no. 5, pp. 2402–2411, Sep. 2014.

[6] H. Sekhavatmanesh, M. Nick, M. Paolone, and R. Cherkaoui, "Service restoration in DG-integrated distribution networks using an exact convex OPF model," in. *Proc. IEEE 20th Power Syst. Comput. Conf.*, 2018, pp. 1–7.

[7] S. Gao, H. Wang, C. Wang, S. Gu, H. Xu, and H. Ma, "Reactive power optimization of low voltage distribution network based on improved particle swarm optimization," in *Proc. IEEE Int. Conf. Elect. Mach. Syst.*, Sydney, NSW, Australia, 2017, pp. 1–5.

[8] L. Franchi, M. Innorta, P. Marannino, and C. Sabelli, "Evaluation of economy and/or security oriented objective functions for reactive power scheduling in large scale systems," *IEEE Trans. Power App. Syst.*, vol. PAS-102, no. 10, pp. 3481–3488, Oct. 1983.

[9] B. Stott, J. Jardim, and O. Alsac, "DC power flow revisited," *IEEE Trans. Power Syst.*, vol. 24, no. 3, pp. 1290–1300, Aug. 2009.

[10] O. Alsac, J. Bright, M. Prais, and B. Stott, "Further developments in LP-based optimal power flow," *IEEE Trans. Power Syst.*, vol. 5, no. 3, pp. 697–711, Aug. 1990.

[11] H. Yuan, F. Li, Y. Wei, and J. Zhu, "Novel linearized power flow and linearized OPF models for active distribution networks with application in distribution LMP," *IEEE Trans. Smart Grid*, vol. 9, no. 1, pp. 438–448, Jan. 2018.

[12] National Academies of Sciences, Engineering, and Medicine, *Analytic Research Foundations for the Next-Generation Electric Grid*. WA, DC, USA: Nat. Academic Press, 2016.

[13] M. Zhao and M. Barati, "Low-order moment relaxation of ACOPF via algorithmic successive linear programming," in *Proc. IEEE Texax Power Energy Conf.*, 2021, pp. 1–6.

[14] H. Zhou, W. Zhang, R. Cong, X. Wu, and X. Zhang, "Optimization of reactive power for active distribution network with power electronic transformer," in *Proc. IEEE 12th Int. Conf. Eur. Energy Market*, Lisbon, Portugal, 2015, pp. 1–5.

[15] S. Li, D. Zhao, Z. Xu, and W. Chao, "Reactive power optimization based on an improved quantum discrete PSO algorithm," in *Proc. IEEE 5th Int. Conf. Crit. Infrastructure*, Beijing, China, 2010, pp. 1–5.

[16] X. Cheng, X. Chen, Y. Fan, Y. Liu, S. Li, and Q. Zhao, "Research on reactive power optimization control strategy of distribution network with photovoltaic generation," in *Proc. IEEE Chin. Autom. Congr.*, Hangzhou, China, 2019, pp. 4026–4030.

[17] D. Zhao, W. Pei, and Z. Xu, "Reactive power optimization by genetic algorithm integrated with reduced gradient method," in *Proc. IEEE Workshop Adv. Res. Technol. Ind. Appl.*, 2014, pp. 838–841.

[18] B. C. Neagu, M. Gavrilaş, and G. G. Matei, "Voltage/VAR control with reactive power injection in distribution networks using a proper metaheuristic approach," in *Proc. IEEE Int. Conf. Environ. Elect. Eng. IEEE Ind. Commercial Power Syst. Eur.*, 2018, pp. 1–6.

[19] Y. Li-min and D. Shu, "Research on reactive power compensation for distribution network based on biogeography-based optimization algorithm," in *Proc. IEEE Int. Conf. Inf. Technol. Electron. Commerce*, 2014, pp. 47–51.

[20] Y. Liu, L. Ma, and J. Zhang, "GA/SA/TS hybrid algorithm for reactive power optimization," in *Proc. IEEE Power Eng. Soc. Summer Meeting*, 2000, vol. 1, pp. 245–249.

[21] Y. Liu, J. Li, and L. Wu, "Distribution system restructuring: Distribution LMP via unbalanced ACOPF," *IEEE Trans. Smart Grid*, vol. 9, no. 5, pp. 4038–4048, Sep. 2018.

[22] Z. Yang, H. Zhong, A. Bose, T. Zheng, Q. Xia, and C. Kang, "A linearized OPF model with reactive power and voltage magnitude: A pathway to improve the MW-only DC OPF," *IEEE Trans. Power Syst.*, vol. 33, no. 2, pp. 1734–1745, Mar. 2018.

[23] C. Yong, Y. Li, Z. Zeng, Z. Zhang, Z. Zhang, and Y. Liu, "Coordinated active and reactive power optimization considering load characteristics for active distribution network," *Chin. J. Elect. Eng.*, vol. 6, no. 4, pp. 97–105, Dec. 2020.

[24] L. R. de Araujo, D. R. R. Penido, and F. de AlcântaraVieira, "A multiphase optimal power flow algorithm for unbalanced distribution systems," *Int. J. Elect. Power Energy Syst.*, vol. 53, pp. 632–642, 2013.

[25] Q. Nguyen, H. V. Padullaparti, K.-W. Lao, S. Santoso, X. Ke, and N. Samaan, "Exact optimal power dispatch in unbalanced distribution systems with high PV penetration," *IEEE Trans. Power Syst.*, vol. 34, no. 1, pp. 718–728, Jan. 2019.

[26] Z. Fan, X. Chang, H. Wang, T. Pu, T. Yu, and G. Liu, "Discrete reactive power optimization based on interior point filter algorithm and complementarity theory," in *Proc. IEEE Int. Conf. Power Syst. Technol.*, 2014, pp. 210–214.

[27] X. Bai and H. Wei, "Semi-definite programming-based method for security-constrained unit commitment with operational and optimal power flow constraints," *IET Gener., Transmiss., Distrib.*, vol. 3, no. 2, pp. 182–197, 2009.

[28] J. Lavaei and S. H. Low, "Zero duality gap in optimal power flow problem," *IEEE Trans. Power Syst.*, vol. 27, no. 1, pp. 92–107, Feb. 2012.

[29] S. Sojoudi and J. Lavaei, "Physics of power networks makes hard optimization problems easy to solve," in *Proc. IEEE Power Energy Soc. Gen. Meeting*, 2012, pp. 1–8.

[30] B. Liu, F. Liu, and S. Mei, "Modeling and analysis of stochastic AC-OPF based on SDP relaxation technique," in *Proc. CCDC*, 2015, pp. 5471–5475.

[31] B. Kocuk, S. S. Dey, and X. A. Sun, "Inexactness of SDP relaxation and valid inequalities for optimal power flow," *IEEE Trans. Power Syst.*, vol. 31, no. 1, pp. 642–651, Jan. 2016.

[32] M. Farivar, R. Neal, C. Clarke, and S. Low, "Optimal inverter VAR control in distribution systems with high PV penetration," in *Proc. IEEE Power Energy Soc. Gen. Meeting*, 2012, pp. 1–7.

[33] Z. Li, W. Wu, X. Tai, and B. Zhang, "A reliability-constrained expansion planning model for mesh distribution networks," *IEEE Trans. Power Syst.*, vol. 36, no. 2, pp. 948–960, Mar. 2021.

[34] A. Merlin and H. Back, "Search for minimum-loss operating spanning tree configuration in an urban power distribution system," in *Proc. 5th Power Syst. Comput. Conf.*, 1975, pp. 1–8.

[35] T.-H. Chen, W.-T. Huang, J.-C. Gu, G.-C. Pu, Y.-F. Hsu, and T.-Y. Guo, "Feasibility study of upgrading primary feeders from radial and open-loop to normally closed-loop arrangement," *IEEE Trans. Power Syst.*, vol. 19, no. 3, pp. 1308–1316, Aug. 2004.

[36] R. Vargas, L. H. Macedo, J. M. Home-Ortiz, J. R. S. Mantovani, and R. Romero, "Optimal restoration of active distribution systems with voltage control and closed-loop operation," *IEEE Trans. Smart Grid*, vol. 12, no. 3, pp. 2295–2306, May 2021.

[37] R. Madani, S. Sojoudi, and J. Lavaei, "Convex relaxation for optimal power flow problem: Mesh networks," *IEEE Trans. Power Syst.*, vol. 30, no. 1, pp. 199–211, Jan. 2015.
[38] M. Farivar and S. H. Low, "Branch flow model: Relaxations and convexification," in *Proc. IEEE Conf. Decis. Control*, 2012, pp. 3672–3679.
[39] R. A. Jabr and I. Dzafic, "A compensation-based conic OPF for weakly meshed networks," *IEEE Trans. Power Syst.*, vol. 31, no. 5, pp. 4167–4168, Sep. 2016.
[40] D. Shirmohammadi, H. Hong, A. Semlyen, and G. Luo, "A compensation-based power flow method for weakly meshed distribution and transmission networks," *IEEE Trans. Power Syst.*, vol. 3, no. 2, pp. 753–762, May 1988.
[41] Y. Liu, J. Li, L. Wu, and T. Ortmeyer, "Chordal relaxation based ACOPF for unbalanced distribution systems with DERs and voltage regulation devices," *IEEE Trans. Power Syst.*, vol. 33, no. 1, pp. 970–984, Jan. 2018.
[42] A. Gabash and P. Li, "Active-reactive optimal power flow in distribution networks with embedded generation and battery storage," *IEEE Trans. Power Syst.*, vol. 27, no. 4, pp. 2026–2035, Nov. 2012.
[43] B. Kocuk, S. S. Dey, and X. A. Sun, "Strong SOCP relaxations for the optimal power flow problem," *Oper. Res.*, vol. 64, no. 6, pp. 1177–1196, 2016.
[44] N. Nazir, P. Racherla, and M. Almassalkhi, "Optimal multi-period dispatch of distributed energy resources in unbalanced distribution feeders," *IEEE Trans. Power Syst.*, vol. 35, no. 4, pp. 2683–2692, Jul. 2020.
[45] B. A. Robbins, H. Zhu, and A. D. Dominguez-Gracia, "Optimal tap setting of voltage regulation transformers in unbalanced distribution systems," *IEEE Trans. Power Syst.*, vol. 31, no. 1, pp. 256–267, Jan. 2016.
[46] G. P. McCormick, "Computability of global solutions to factorable nonconvex programs: Part I—convex underestimating problems," *Math. Prog.*, vol. 10, pp. 147–175, 1976.
[47] W. C. Wu and B. M. Zhang, "A three-phase power flow algorithm for distribution system power flow based on loop-analysis method," *Int. J. Elect. Power Energy Syst.*, vol. 30, pp. 8–15, 2008.
[48] S. K. Goswami and S. K. Basu, "A new algorithm for the reconfiguration of distribution feeders for loss minimization," *IEEE Trans. Power Del.*, vol. 7, no. 3, pp. 1484–1491, Jul. 1992.
[49] J. S. Savier and D. Das, "Impact of network reconfiguration on loss allocation of radial distribution systems," *IEEE Trans. Power Del.*, vol. 22, no. 4, pp. 2473–2480, Oct. 2007.
[50] D. Zhang, Z. Fu, and L. Zhang, "An improved TS algorithm for loss-minimum reconfiguration in large-scale distribution systems," *Elect. Power Syst. Res.*, vol. 77, no. 5-6, pp. 685–694, 2007.
[51] J. R. S. Mantovani, F. Casari, and R. A. Romero, "Reconfiguração de sistemas de distribuição radiais utilizando o criteŕio de queda de tensão," *SBA: Controle Automação*, vol. 11, no. 3, pp. 150–159, Dec. 2000.
[52] H. M. Khodr, F. G. Olsina, P. M. De Oliveira-De Jesus, and J. M. Yusta, "Maximum savings approach for location and sizing of capacitors in distribution systems," *Elect. Power Syst. Res.*, vol. 78, no. 7, pp. 1192–1203, Jul. 2008.
[53] W. H. Kersting, "Radial distribution test feeders," in *Proc. IEEE Power Eng. Soc. Winter Meeting*, 2001, vol. 2, pp. 908–912.
[54] T. Xu and T. Ding, "System_906," 2022. [Online]. Available: https://github.com/TianruiXu/system_906
[55] Gurobi. [Online]. Available: http://www.gurobi.com/
[56] S. K. Goswami and S. K. Basu, "Direct solution of distribution systems," *Proc. Inst. Elect. Eng. C*, vol. 138, no. 1, pp. 78–88, Jan. 1991.

Tianrui Xu (Student Member, IEEE) received the B.S. degree, in 2020, from the School of Electrical Engineering, Xi'an Jiaotong University, Xi'an, China, where he is currently working toward the M.S. degree. His main research interests include distribution system and power system optimization.

Tao Ding (Senior Member, IEEE) received the B.S.E.E. and M.S.E.E. degrees from Southeast University, Nanjing, China, in 2009 and 2012, respectively, and the Ph.D. degree from Tsinghua University, Beijing, China, in 2015. During 2013–2014, he was a Visiting Scholar with the Department of Electrical Engineering and Computer Science, University of Tennessee, Knoxville, TN, USA. During 2019–2020, he was a Visiting Scholar with the Robert W. Galvin Center for Electricity Innovation, Illinois Institute of Technology, Chicago, IL, USA. He is currently a Professor with the State Key Laboratory of Electrical Insulation and Power Equipment, School of Electrical Engineering, Xi'an Jiaotong University, Xi'an, China. His current research interests include electricity markets, power system economics and optimization methods, and power system planning and reliability evaluation. He is the Editor of IEEE TRANSACTIONS ON POWER SYSTEMS, IEEE POWER ENGINEERING LETTERS, IEEE SYSTEMS JOURNAL, *IET Generation Transmission & Distribution*, and *CSEE JPES*.

Chenggang Mu (Student Member, IEEE) received the B.S. degree from the School of Electrical Engineering, Xi'an Jiaotong University, Xi'an, China, in 2021, where he is currently working toward the Ph.D. degree. His main research interests include power system optimization and electricity markets.

Yuntao Ju (Member, IEEE) received the B.Sc. degree in mechanical engineering and the Ph.D. degree in electrical engineering from Tsinghua University, Beijing, China, in 2008 and 2013, respectively. In 2013, he was a Visiting Scholar with the University of Toronto. In 2015, he joined China Electric Power Research Institute as a Research Fellow. He is currently an Associate Professor with the College of Information and Electrical Engineering, China Agricultural University, Beijing, China. His research interests include hybrid energy system modeling, high-speed dynamic simulation, large-scale system parameter identification, state estimation, and uncertainty optimization. He was an awardee of excellent graduates from Tsinghua University in 2008.

Mohammad Shahidehpour (Fellow, IEEE) received the Honorary Doctorate degree from the Polytechnic University of Bucharest, Bucharest, Romania, in 2009. He is currently a University Distinguished Professor, Bodine Chair Professor, and the Director of the Robert W. Galvin Center for Electricity Innovation, Illinois Institute of Technology, Chicago, IL, USA. He is a Member of the U.S. National Academy of Engineering, and a Fellow of the American Association for the Advancement of Science (AAAS) and the National Academy of Inventors (NAI).

Chao Zhu reveiced the B.S. and Ph.D. degrees from the School of Energy and Power Engineering, Xi'an Jiaotong University, Xi'an, China, in 2012 and 2017, respectively. His current research interests include integrated demand response research, deep-peak shaving, energy storage, and geothermal energy.

Yiyang Zhang received the B.S. and M.S. degrees from the School of Electrical Engineering, Chongqing University, Chongqing, China, in 2009 and 2012, respectively. His current research interests include power system stability analysis and wind power prediction research.